CMOS-compatible temperature-independent tunable silicon optical lattice filters

Liangjun Lu, Linjie Zhou,* Xiaomeng Sun, Jingya Xie, Zhi Zou, Haike Zhu, Xinwan Li, and Jianping Chen

State Key Laboratory of Advanced Optical Communication Systems and Networks, Department of Electronic Engineering, Shanghai Jiao Tong University, Shanghai, 200240, China
ljzhou@sjtu.edu.cn

Abstract: We present a CMOS-compatible athermal tunable silicon optical lattice filter composed of 10 cascaded 2 × 2 asymmetric Mach-Zehnder interferometers. Active tuning experiments show that the filter central wavelength can be red-/blue-shifted by 13.1/21.3 nm with power consumption of 77/96 mW on top/bottom arms. Temperature shift measurements show that the thermal-sensitivity of the filter central wavelength before active tuning is as low as −1.465 pm/°C. The thermal-sensitivity is varied within 26.5 pm/°C to −27.1 pm/°C when the filter central wavelength is tuned in the wavelength range of 1534 nm to 1551 nm. We use the transfer matrix method to theoretically model the lattice filter and its thermal-sensitivity before and after tuning is analyzed and discussed.

OCIS codes: (130.3120) Integrated optics devices; (130.7408) Wavelength filtering devices; (230.7408) Wavelength filtering devices.

References and links

1. G. T. Reed, "Device physics: the optical age of silicon," Nature **427**(6975), 595–596 (2004).
2. S. Fathpour, *Silicon Photonics for Telecommunications and Biomedicine* (CRC Press, 2011).
3. R. Soref, "The past, present, and future of silicon photonics," IEEE J. Sel. Top. Quantum Electron. **12**(6), 1678–1687 (2006).
4. H. H. Li, "Refractive index of silicon and germanium and its wavelength and temperature derivatives," J. Phys. Chem. Ref. Data **9**(3), 561–601 (1980).
5. B. J. Frey, D. B. Leviton, and T. J. Madison, "Temperature-dependent refractive index of silicon and germanium," Proc. SPIE **6273**, 62732J, 62732J-10 (2006).
6. B. Guha, B. B. C. Kyotoku, and M. Lipson, "CMOS-compatible athermal silicon microring resonators," Opt. Express **18**(4), 3487–3493 (2010).
7. M. Uenuma and T. Moooka, "Temperature-independent silicon waveguide optical filter," Opt. Lett. **34**(5), 599–601 (2009).
8. M. R. Watts, W. A. Zortman, D. C. Trotter, G. N. Nielson, D. L. Luck, and R. W. Young, "Adiabatic resonant microrings (ARMs) with firectly integrated thermal microphotonics," in *Conference on Lasers and Electro-Optics/International Quantum Electronics Conference*, OSA Technical Digest (CD) (Optical Society of America, 2009), paper CPDB10.
9. C. Qiu, J. Shu, Z. Li, X. Zhang, and Q. Xu, "Wavelength tracking with thermally controlled silicon resonators," Opt. Express **19**(6), 5143–5148 (2011).
10. K. Padmaraju, J. Chan, L. Chen, M. Lipson, and K. Bergman, "Thermal stabilization of a microring modulator using feedback control," Opt. Express **20**(27), 27999–28008 (2012).
11. J. Teng, P. Dumon, W. Bogaerts, H. Zhang, X. Jian, X. Han, M. Zhao, G. Morthier, and R. Baets, "Athermal Silicon-on-insulator ring resonators by overlaying a polymer cladding on narrowed waveguides," Opt. Express **17**(17), 14627–14633 (2009).
12. P. Alipour, E. S. Hosseini, A. A. Eftekhar, B. Momeni, and A. Adibi, "Athermal performance in high-Q polymer-clad silicon microdisk resonators," Opt. Lett. **35**(20), 3462–3464 (2010).
13. L. Wang, W. Bogaerts, P. Dumon, S. K. Selvaraja, G. Morthier, J. Teng, X. Han, X. Jian, M. Zhao, and R. Baets, "Athermal AWGs in SOI by overlaying a polymer cladding on narrowed arrayed waveguides," in *Optical Fiber Communication Conference*, OSA Technical Digest (CD) (Optical Society of America, 2011), paper OThV6.

#183887 - $15.00 USD Received 22 Jan 2013; revised 14 Mar 2013; accepted 26 Mar 2013; published 9 Apr 2013

14. L. Zhou, K. Okamoto, and S. J. B. Yoo, "Athermalizing and trimming of slotted silicon microring resonators with UV-sensitive PMMA upper-cladding," IEEE Photon. Technol. Lett. **21**(17), 1175–1177 (2009).
15. B. Guha, A. Gondarenko, and M. Lipson, "Minimizing temperature sensitivity of silicon Mach-Zehnder interferometers," Opt. Express **18**(3), 1879–1887 (2010).
16. B. Guha, K. Preston, and M. Lipson, "Athermal silicon microring electro-optic modulator," Opt. Lett. **37**(12), 2253–2255 (2012).
17. K. Yamada, T. Shoji, T. Tsuchizawa, T. Watanabe, J.-i. Takahashi, and S.-i. Itabashi, "Silicon-wire-based ultrasmall lattice filters with wide free spectral ranges," Opt. Lett. **28**(18), 1663–1664 (2003).
18. W. Qian and H. Sailing, "Optimal design of planar wavelength circuits based on Mach-Zehnder interferometers and their cascaded forms," J. Lightwave Technol. **23**(3), 1284–1290 (2005).
19. S. S. Djordjevic, L. W. Luo, S. Ibrahim, N. K. Fontaine, C. B. Poitras, B. Guan, L. Zhou, K. Okamoto, Z. Ding, M. Lipson, and S. J. B. Yoo, "Fully reconfigurable silicon photonic lattice filters with four cascaded unit cells," IEEE Photon. Technol. Lett. **23**(1), 42–44 (2011).
20. S. Ibrahim, N. K. Fontaine, S. S. Djordjevic, B. Guan, T. Su, S. Cheung, R. P. Scott, A. T. Pomerene, L. L. Seaford, C. M. Hill, S. Danziger, Z. Ding, K. Okamoto, and S. J. B. Yoo, "Demonstration of a fast-reconfigurable silicon CMOS optical lattice filter," Opt. Express **19**(14), 13245–13256 (2011).
21. C. Li, J. H. Song, J. Zhang, H. Zhang, S. Chen, M. Yu, and G. Q. Lo, "Silicon polarization independent microring resonator-based optical tunable filter circuit with fiber assembly," Opt. Express **19**(16), 15429–15437 (2011).
22. M. J. Strain, M. Gnan, G. Bellanca, R. M. De La Rue, and M. Sorel, "Retrieval of bragg grating transmission spectra by post-process removal of spurious Fabry-Pérot oscillations," Opt. Express **17**(16), 13493–13501 (2009).
23. C. K. Madsen and J. H. Zhao, *Optical Filter Design and Analysis* (John Wiley & Sons, Inc., 1999).

1. Introduction

Silicon photonics has become one of the most promising optical platforms for future optical communication and interconnect applications, because of their large refractive index contrast and compatibility with the standard complementary metal-oxide-semiconductor (CMOS) technologies [1–3]. However, high temperature sensitivity is one of the fundamental limitations for silicon photonic devices, as silicon has a large thermo-optic (TO) coefficient of ~1.86×10^{-4}/°C around 1.55 μm wavelength [4, 5]. Indeed, silicon photonic devices suffer from a relatively large thermal shift upon temperature variation. For example, silicon ring resonators have a temperature sensitivity of ~110 pm/°C [6]. Silicon Mach-Zehnder interferometers (MZIs) and arrayed waveguide gratings (AWGs) show a temperature dependent wavelength shift of about 80 pm/°C [7].

Several approaches have been proposed to reduce the temperature sensitivity. One of the proposed methods is to use local heating to get active thermal stabilization subjected to thermally volatile environment [8–10], but it requires a complex system with extra power consumption. Another approach is to overlay a polymer cladding with negative TO coefficient on the devices to compensate the positive TO coefficient of silicon [11–14]. In order to achieve athermal operation, more light should be localized out of the silicon core into the polymer cladding. However, reducing the dimension of silicon waveguide increases the challenge on fabrication. Moreover, polymers are currently not compatible with the CMOS technologies, and the reliability of polymer materials at higher temperatures is a big issue. One passive and CMOS-compatible solution is to use asymmetric MZI structures, which have been theoretically analyzed and experimentally demonstrated in silicon MZIs [7, 15] and ring resonators [6, 16].

In this paper, we present a CMOS-compatible temperature-independent tunable silicon optical lattice filter constituted by 10 cascaded athermal MZIs. Lattice filters are widely adopted for (de)multiplexing and dispersion compensation with the advantages of flexible design and large free spectral range (FSR) [17–20]. Compared with a single MZI, lattice filters have the advantages of narrower passband and faster passband roll-off. Our tunable optical lattice filter shows a wide wavelength tuning range and low temperature sensitivity around 1.55 μm wavelength.

#183887 - $15.00 USD Received 22 Jan 2013; revised 14 Mar 2013; accepted 26 Mar 2013; published 9 Apr 2013

2. Device structure and fabrication

Figure 1(a) shows the optical microscope image of the fabricated device, which consists of 10 cascaded 2 × 2 MZIs. Figure 1(b) shows the magnified asymmetric MZI unit with the arm waveguide width and length labeled in the graph. As the guided modes in the two arms have different effective TO coefficients due to their different waveguide widths, the temperature-induced phase shifts can be canceled by properly choosing the lengths of the MZI arms. In our design, we set the central wavelength of the lattice filter at 1.55 μm wavelength with an athermal operation. The waveguides are 220 nm high with a 60 nm slab. The narrow waveguide (350 nm wide) in the top arm is connected with 4-μm-long tapers to regular waveguides (500 nm wide). The gap size of the 2 × 2 couplers is 0.25 μm.

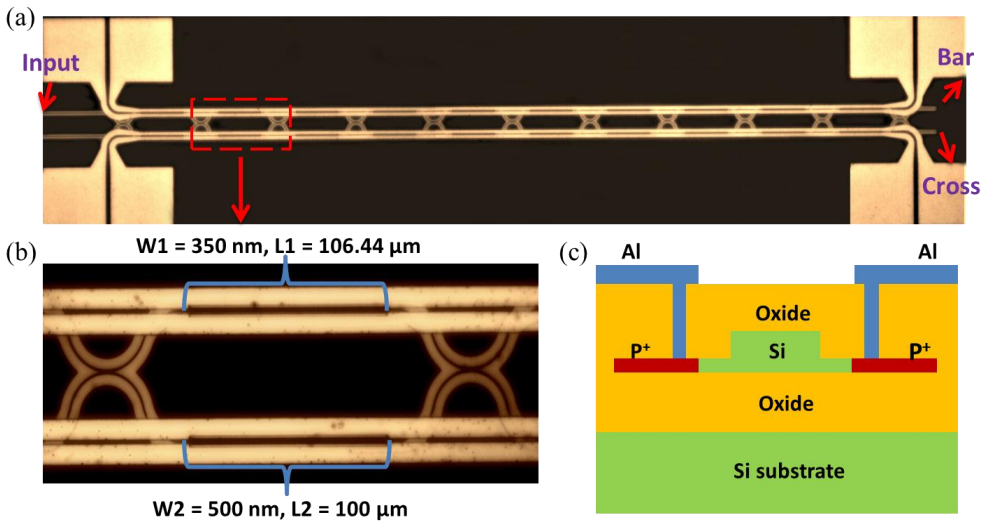

Fig. 1. (a) Microscope image of the tunable silicon optical lattice filter. (b) Zoom-in view of one MZI stage. (c) Cross-sectional schematic of the p-i-p junction-based micro-heater.

Phase shifters for active tuning are embedded in both top and bottom arms. The phase shifters are composed of lateral p-i-p junctions as schematically shown in Fig. 1(c). The two highly doped P^+ regions are separated by 600 nm away from the edges of the ridge waveguide to avoid extra loss caused by free carrier absorption. The intrinsic region has a high resistivity and works as a micro-heater. It should be noted that the p-i-p junction is not a diode but a resistor in essence. When current flows through the resistor, heat will be generated therein and yet the free-carrier absorption loss does not increase significantly. Our calculation shows that a refractive index change of 0.008 only causes the free-carrier absorption loss to increase from 0.042 dB/cm to 0.157 dB/cm, which is much smaller than the p-i-n diode based tuning approach. As it is the waveguide that makes up the resistor, the generated heat directly interacts with the optical mode. There is no heat diffusion process as in a conventional thermal tuning structure where a metal heater is put on top of the waveguide [21]. Our simulation shows that this type of p-i-p resistive micro-heaters has a higher tuning efficiency and a faster temporal response than conversional structures. Moreover, the fabrication of p-i-p resistors is compatible with that of p-i-n or p-n diodes routinely used for electrical tuning of silicon waveguides, without adding complexity to fabrication process.

The device was fabricated on a silicon-on-isolator (SOI) wafer with a top silicon layer thickness of 220 nm and a buried oxide layer thickness of 2 μm. The top silicon layer has a resistivity of 10 to 15 Ohm·cm (corresponding to a hole concentration of ~10^{15} cm^{-3}). The

#183887 - $15.00 USD Received 22 Jan 2013; revised 14 Mar 2013; accepted 26 Mar 2013; published 9 Apr 2013

wafer was patterned by 248-nm deep ultra-violet (DUV) photolithography and plasma dry etched with an etched depth of ~160 nm to transfer the patterns onto the top silicon layer. Consequently, ion implantation of boron was used to form the P^+ doped regions with a concentration of ~10^{20} cm^{-3} for ohmic contact. After depositing a 1.5 μm thick silicon dioxide layer using plasma-enhanced chemical vapor deposition (PECVD) as the device upper-cladding, contact holes were etched through. Electrical connection was finally formed by sputtering of aluminum and dry etch.

3. Experiments

We used the Agilent loss and dispersion analyzer (86038B) to characterize the device transmission performances. Light was coupled into and out of the device through on-chip inverse tapers with a tip width of 180 nm. The active tuning of the device was performed by connecting an external current source to the p-i-p resistor via a pair of metal probes. In order to accurately tune and monitor the device temperature, a thermoelectric cooler (TEC) and a temperature sensor were put under the chip during the device thermal-sensitivity measurement.

3.1 Active tuning measurement

Figure 2 shows the measured transmission spectra of the lattice filter with tuning performed to the top and bottom arms of the MZIs. The extinction ratio of the filter stopband in the bar-port is ~10.1 dB. The extinction ratio of the filter passband in the cross-port, which is defined as the intensity difference between the main peak and the first sidelobe, is ~7.2 dB. The 3-dB bandwidth of the device is ~7.24 nm. There is only one filtering band observed over the measured spectral range from 1495 nm to 1640 nm before active tuning. Another filtering band could be observed when the bottom arm is tuned with an electrical tuning power of ~96 mW as seen from Figs. 2(d) and 2(e), so the device FSR is larger than 112 nm in the spectral range of interest. Figures 2(c) and 2(f) show the extracted filter central wavelength changing as a function of electrical tuning power applied to the top and bottom arms, respectively. The filter central wavelength shifts by 13.1 nm to the longer wavelength side when the top arms are tuned with a power consumption of ~77 mW. The power tuning efficiency is 0.17 nm/mW. In contrast, the filter spectrum shifts by 21.3 nm to the shorter wavelength side when the bottom arms are tuned with a power consumption of ~96 mW. The power tuning efficiency is 0.22 nm/mW, higher than the previous case. The difference in the tuning efficiency is probably due to the difference in contact resistance of the top and bottom arms. The extinction ratio slightly changes upon tuning since the coupling coefficient of the 2 × 2 couplers is wavelength dependent. It is also observed that Fabry-Pérot (FP) like fringes appear in the spectrum when the applied electric current becomes large. From the FSR of the FP fringes, we infer that the FP oscillations are generated because of the increased waveguide refractive index of the phase shifters when they are heated up [22].

3.2 Thermal-sensitivity measurement

Figure 3 shows the measured transmission spectra of the lattice filter at various temperatures without tuning. The spectrum blueshifts with the increasing temperature at the longer wavelength side (close to 1.64 μm), while it slightly redshifts at the shorter wavelength side (close to 1.5 μm). The temperature insensitive operation window is around 1.546 μm as seen from Figs. 3(c) and 3(d). By linear fitting the filter central wavelength shift with temperature, the thermal-sensitivity $d\lambda_0/dT$ of the lattice filter can be extracted to be −1.465 pm/°C. It is more than one order smaller than that of regular silicon optical filters. It should be noted that, although the filter central wavelength is almost temperature independent, it can still be thermally tuned by locally heating the top or bottom arms of the lattice filter as shown in Fig. 2.

#183887 - $15.00 USD Received 22 Jan 2013; revised 14 Mar 2013; accepted 26 Mar 2013; published 9 Apr 2013

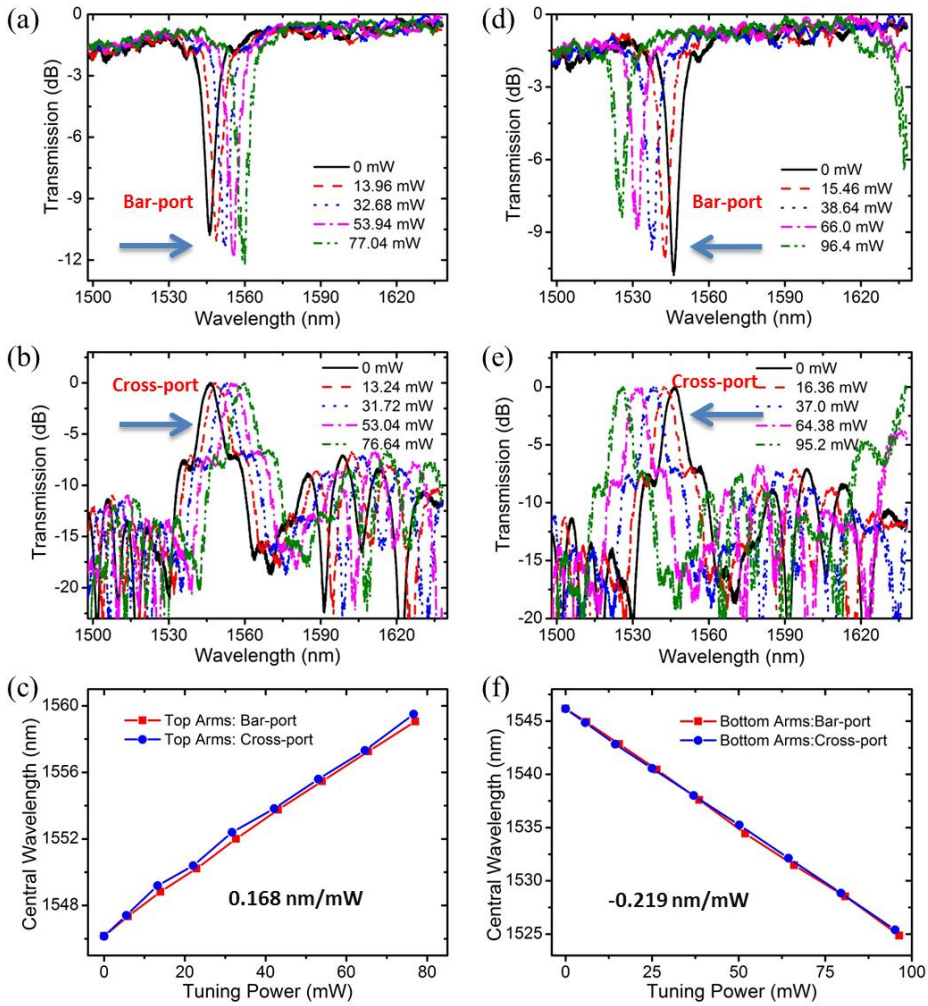

Fig. 2. Transmission spectrum and filter central wavelength change with the tuning power. (a)-(c) Power is applied to the top arms. (d)-(f) Power is applied to the bottom arms.

We also characterized the device thermal-sensitivity after the filter was tuned by an electric current. Figure 4(a) shows the filter central wavelength shifts with temperature. The central wavelength is tuned to various wavelengths under appropriate tuning powers as represented by the six groups of horizontal lines in Fig. 4(a). We can see that the thermal shift of the filter central wavelength is wavelength dependent. As the athermal operation window is around 1.546 μm, the thermal shift reaches the minimum around that wavelength. When the central wavelength is tuned to a shorter wavelength, it redshifts with the temperature where the MZI phases are under-compensated. In contrast, at a longer wavelength, the MZI phases are over-compensated leading to a blueshift instead. The extracted thermal-sensitivity of the filter varies from 26.5 pm/°C to –27.1 pm/°C, when the central wavelength is tuned in the wavelength range from 1534 nm to 1551 nm as illustrated in Fig. 4(b).

#183887 - $15.00 USD Received 22 Jan 2013; revised 14 Mar 2013; accepted 26 Mar 2013; published 9 Apr 2013

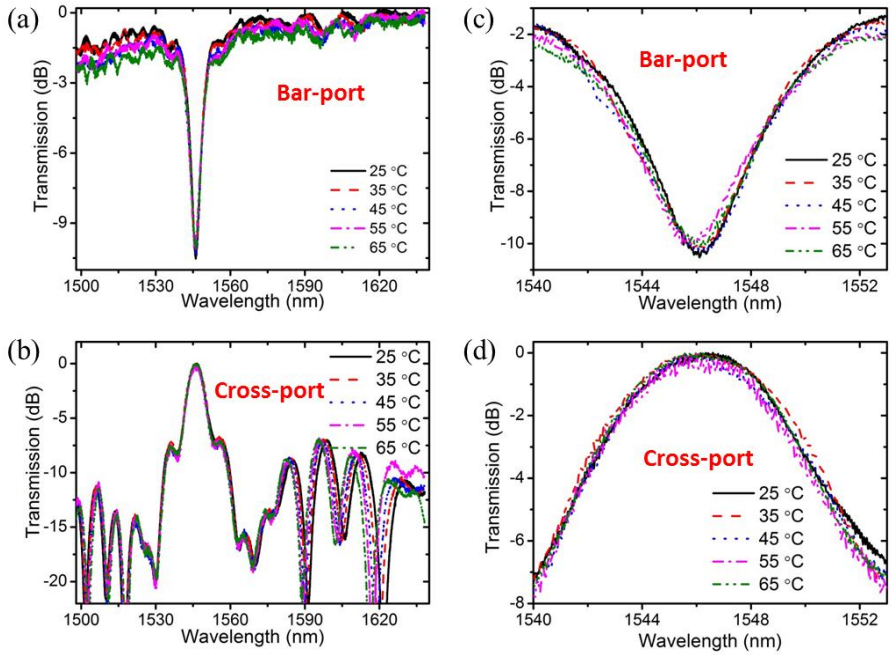

Fig. 3. (a) and (b) Thermal shift of the lattice filter transmission spectra in response to increased temperature. (c) and (d) Zoom-in view of the filtering band.

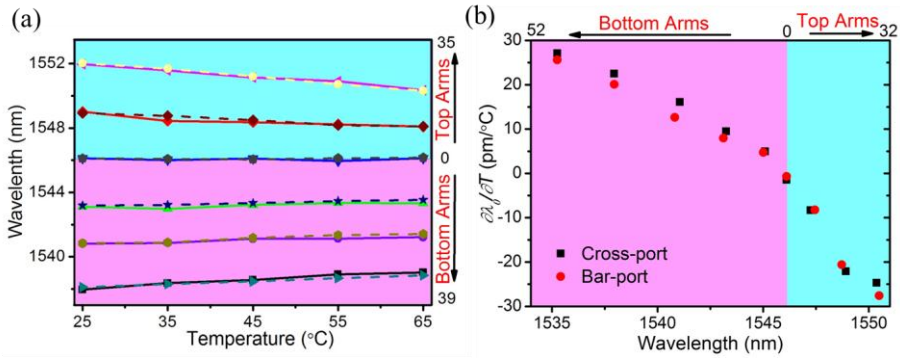

Fig. 4. (a) Thermal shift of the filter central wavelength with temperature. The different lines indicate the shifted central wavelengths under appropriate tuning powers. Solid lines: bar-port; dashed lines: cross-port. (b) Variation of the thermal-sensitivity when the filter central wavelength is actively tuned.

4. Analysis and discussion

MZI-based optical filters have two asymmetric arms with unequal optical lengths. The phase difference of an asymmetric MZI is given by

$$\Delta\phi = \frac{2\pi}{\lambda}(n_{eff\,1}L_1 - n_{eff\,2}L_2), \tag{1}$$

where n_{effi} (i = 1, 2 for top and bottom arms, respectively) is the MZI arm waveguide effective refractive index, L_i is the corresponding arm length, and λ is the wavelength. The filter central wavelength λ_0 satisfies $\Delta\phi$ (λ_0) = $2m\pi$, where m is an integer. The FSR of the MZI is given by

#183887 - $15.00 USD Received 22 Jan 2013; revised 14 Mar 2013; accepted 26 Mar 2013; published 9 Apr 2013

$$FSR = \frac{\lambda_0^2}{n_{g1}L_1 - n_{g2}L_2}, \tag{2}$$

where n_{gi} is the MZI arm waveguide group refractive index. A large FSR could be achieved when the length difference of these two arms is small. However, optical filters based on one single MZI usually have a large bandwidth and a slow roll-off [15]. Lattice filters consisting of cascaded MZIs could narrow the filter bandwidth and sharpen the passband roll-off [23]. Indeed, our calculation shows that the single-stage MZI as used in our lattice filter exhibits almost no pronounced passband in the cross-port. When the number of stages increases from 4 to 10, the filter bandwidth decreases from 6.6 nm to 4.9 nm with a sharper roll-off.

Temperature variation changes the phase difference of the two arms, which causes a spectral shift of the filter passband. The temperature sensitivity of the phase difference is given by

$$\frac{\partial \Delta\phi}{\partial T} = \frac{2\pi}{\lambda}\left(\frac{\partial n_{eff\,1}}{\partial T}L_1 - \frac{\partial n_{eff\,2}}{\partial T}L_2\right), \tag{3}$$

where $\partial n_{effi}/\partial T$ is the effective TO coefficient of the MZI arm waveguide. The effective TO coefficient is dependent on the waveguide geometry, so variation in either the waveguide height or width can change it [7, 15].

Because it is easy to design waveguides with different widths, we can cancel the temperature-induced phase shift by carefully choosing the waveguide width and length of each MZI unit. We numerically solve the silicon ridge waveguide mode using the finite element method (FEM). The waveguide height is fixed at 220 nm. The TO coefficient of Si and SiO_2 are chosen as 1.86×10^{-4}/°C and 1.0×10^{-5}/°C, respectively. Figure 5(a) shows the calculated $\partial n_{eff}/\partial T$ at 1.55 μm wavelength as a function of waveguide width. We can see that $\partial n_{eff}/\partial T$ changes substantially when the waveguide width varies from 280 nm to 540 nm. When the waveguide width exceeds 540 nm, $\partial n_{eff}/\partial T$ only slightly changes. Figure 5(b) shows the sensitivity of phase difference as a function of MZI top arm waveguide width. The bottom arm width is fixed at 500 nm. We can see that $\partial\Delta\phi/\partial T$ changes from negative to positive with the increasing waveguide width. When the width is close to 350 nm, which is our design, $\partial\Delta\phi/\partial T$ is zero and the MZI satisfies the athermal condition.

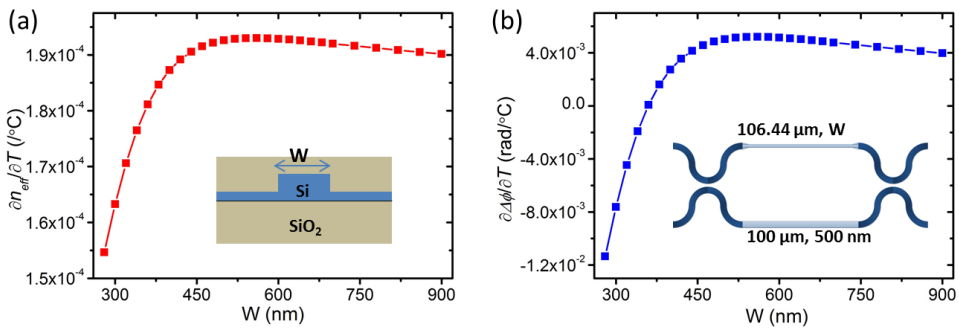

Fig. 5. Simulated temperature sensitivities of (a) the effective index of the silicon ridge waveguide and (b) the phase difference of the asymmetric MZI as a function of top arm waveguide width.

The field transmission in the lattice filter can be modeled by using the transfer matrix method. The transmitted electric fields at the bar and cross ports are given by:

#183887 - $15.00 USD Received 22 Jan 2013; revised 14 Mar 2013; accepted 26 Mar 2013; published 9 Apr 2013

$$\begin{pmatrix} E_{bar} \\ E_{cross} \end{pmatrix} = (M_c M_{arm})^{10} M_c \begin{pmatrix} E_{in} \\ 0 \end{pmatrix}$$
$$= \left(\begin{bmatrix} t & -i\kappa \\ -i\kappa & t \end{bmatrix} \begin{bmatrix} \exp(-i\phi_1) & 0 \\ 0 & \exp(-i\phi_2) \end{bmatrix} \right)^{10} \begin{bmatrix} t & -i\kappa \\ -i\kappa & t \end{bmatrix} \begin{pmatrix} E_{in} \\ 0 \end{pmatrix}, \quad (4)$$

where t and κ are the transmission and coupling coefficients of the 2 × 2 couplers, $\phi_i = (2\pi/\lambda)n_{effi}L_i$ is the optical phase of the MZI arm. The phase difference is then given by $\Delta\phi = \phi_1 - \phi_2$.

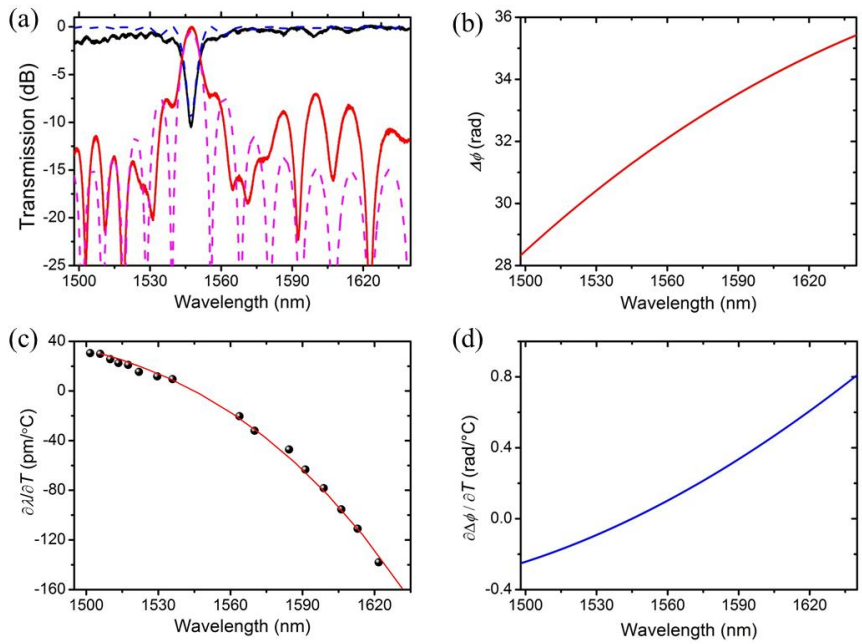

Fig. 6. (a) Measured (solid line) and fitted (dashed line) transmission spectra without active tuning. (b) Extracted phase difference between MZI arms as a function of wavelength. (C) Measured (solid symbols) and fitted (red line) thermal-sensitivity of the lattice filter. (d) Extracted temperature sensitivity of phase difference as a function of wavelength.

It is the phase difference $\Delta\phi$ between the MZI two arms that determines the device transmission spectra. Due to various fabrication errors in photolithography and dry etch, the real dimensions of the top and bottom arm waveguides are always slightly deviated from the designed values. Indeed, a fabrication error of only several nanometers in arm waveguide width can cause a transmission spectrum shift of dozens of nanometers. The variation in coupling coefficient also affects the extinction ratio of the filter. We use Eq. (4) to calculate the transmission spectra of the device as shown by the dashed lines in Fig. 6(a). The coupling coefficient of the couplers is κ = 0.173 and $\Delta\phi$ is a fitting parameter with a quadratic dependence on wavelength as shown in Fig. 6(b). Comparing the fitted and measured spectra, we can see that the wavelengths of the main peak and sidelobes are well matched. The deviation in the spectral profile is probably caused by the non-uniform phase errors and coupling coefficients of the 10 MZI units.

The fabrication error of several nanometers in arm waveguide width can also deteriorate the temperature sensitivity of the lattice filter by tens of pm/°C. From the thermal shift measurement of the cross-port (see Fig. 3(b)), we can extract the thermal-sensitivity ($\partial\lambda/\partial T$) of the main and sidelobe peaks as shown by the solid dots in Fig. 6(c). With Eq. (4) and

#183887 - $15.00 USD Received 22 Jan 2013; revised 14 Mar 2013; accepted 26 Mar 2013; published 9 Apr 2013

considering the temperature dependence of $\Delta\phi$ as $\Delta\phi(T) = \Delta\phi(T_0) + (T-T_0)\partial\Delta\phi/\partial T$, we can calculate the spectrum shift with temperature and thus the thermal-sensitivity at each wavelength. Assuming $\partial\Delta\phi/\partial T$ is a quadratic function of wavelength, the fitted thermal-sensitivity curve is shown by the red curve in Fig. 6(c). Figure 6(d) shows the wavelength dependent $\partial\Delta\phi/\partial T$ used in fitting.

The thermal-sensitivity of the filter central wavelength λ_0 is given by [7, 15]

$$\frac{\partial\lambda_0}{\partial T} = \frac{\dfrac{\partial\Delta\phi(\lambda_0)}{\partial T}\Big/\dfrac{2\pi}{\lambda_0}}{M(\lambda_0)} = \frac{\dfrac{\partial\Delta\phi(\lambda_0)}{\partial T}\Big/\dfrac{2\pi}{\lambda_0}}{m - \dfrac{\partial\Delta\phi(\lambda_0)}{\partial\lambda}\Big/\dfrac{2\pi}{\lambda_0}}, \tag{5}$$

where M is the interference order incorporating the wavelength-dispersion effect, and $\partial\Delta\phi(\lambda_0)/\partial\lambda$ is the first-order derivative of the phase difference with respect to wavelength. Using the extracted $\Delta\phi$ and $\partial\Delta\phi/\partial T$ (see Fig. 6), we can obtain the thermal-sensitivity of the filter central wavelength after tuning as shown in Fig. 7. It should be noted that here we only concern the thermal-sensitivity of the central wavelength upon active tuning. The thermal-sensitivity does not linearly change with the central wavelength, because of the nonlinearity of $\Delta\phi$ and $\partial\Delta\phi/\partial T$. The calculated thermal-sensitivity is changed from 11.7 pm/°C to −7.2 pm/°C in the wavelength range of 1534 nm to 1551 nm. However, the measured one is changed from 26.5 pm/°C to −27.1 pm/°C (see Fig. 4(b)). The main reason is that the applied power on the device decreases with the rising temperature (due to the p-i-p type resistor), although we use a constant electric current source. For instance, when we apply 2 mA current to the bottom arms, the monitored voltage decreases from 8.75 V to 7.67 V when the temperature rises from 25 °C to 45 °C. When the filter passband is tuned to the longer wavelength side, it is over-compensated resulting in a blueshift of the central wavelength with the rising temperature. Meanwhile, the power supplied to the device is reduced due to the increased temperature, which in turn further blueshifts the central wavelength. As a result, the measured thermal-sensitivity of the central wavelength is larger than the calculated value. Similar scenario occurs when the central wavelength is tuned to the shorter wavelength side.

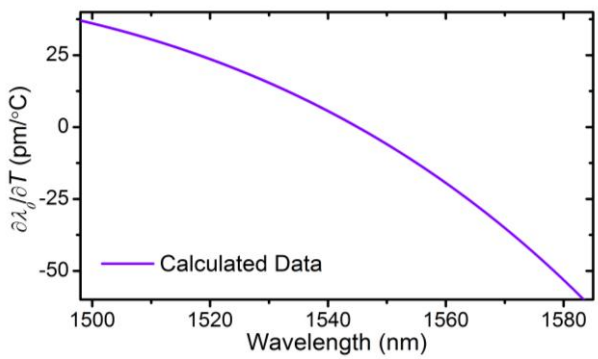

Fig. 7. Calculated thermal-sensitivity of the lattice filter changing with its central wavelength.

5. Conclusions

CMOS-compatible athermal tunable silicon optical lattice filters were proposed, fabricated and experimentally demonstrated. Experimental results show that the filter central wavelength can be redshifted by 13.1 nm (power consumption 77 mW) with a power tuning efficiency of 0.17 nm/mW, and blueshifted by 21.3 nm (power consumption 96 mW) with a power tuning efficiency of 0.22 nm/mW. Temperature sensitivity measurements show that

#183887 - $15.00 USD Received 22 Jan 2013; revised 14 Mar 2013; accepted 26 Mar 2013; published 9 Apr 2013

the thermal-sensitivity of the filter without active tuning is −1.465 pm/°C, improved by more than one order compared to regular designs. When the filter central wavelength is tuned in between 1534 nm to 1551 nm, the measured thermal-sensitivity varies from 26.5 pm/°C to −27.1 pm/°C. Using the transfer matrix method, we modeled the lattice filter and its transmission spectra were compared with experiments. The thermal sensitivity before and after tuning was also analyzed and discussed in detail.

Acknowledgments

This work was supported in part by the 973 program (ID2011CB301700), the 863 program (2013AA014402), the National Natural Science Foundation of China (NSFC) (61007039, 61001074, 61127016), the Science and Technology Commission of Shanghai Municipality (STCSM) Project (10DJ1400402, 12XD1406400). We also acknowledge IME Singapore for device fabrication.

#183887 - $15.00 USD Received 22 Jan 2013; revised 14 Mar 2013; accepted 26 Mar 2013; published 9 Apr 2013